American Mineralogist, Volume 88, pages 967–977, 2003

XANES calibrations for the oxidation state of iron in a silicate glass

ANDREW J. BERRY,[1,*] HUGH ST.C. O'NEILL,[1] KASTHURI D. JAYASURIYA,[2,†] STEWART J. CAMPBELL,[2] AND GARRY J. FORAN[3,4]

[1]Research School of Earth Sciences, Australian National University, Canberra, ACT 0200, Australia
[2]School of Physics, University of New South Wales, Australian Defence Force Academy, Canberra, ACT 2600, Australia
[3]Australian Synchrotron Research Program, Australian Nuclear Science and Technology Organization, PMB 1, Menai, NSW 2234, Australia
[4]Australian National Beamline Facility, KEK, Photon Factory, Oho 1-1, Tsukuba-shi, Ibaraki-ken 305-0801, Japan

ABSTRACT

Fe *K*-edge X-ray absorption near edge structure (XANES) spectra were recorded for a series of anorthite-diopside eutectic glasses containing 1 wt% $^{57}Fe_2O_3$ quenched from melts equilibrated over a range of oxygen fugacities at 1409 °C. The $Fe^{3+}/\Sigma Fe$ ratios were determined previously by ^{57}Fe Mössbauer spectroscopy and vary between 0 (fully reduced) and 1 (fully oxidized). Using the Mössbauer results as a reference, various methods for extracting $Fe^{3+}/\Sigma Fe$ ratios from XANES spectra were investigated. The energy of the $1s \rightarrow 3d$ pre-edge transition centroid was found to correlate linearly with the oxidation state. Correlations also exist with the energy of the *K* absorption edge and the area of peaks in the derivative spectrum associated with the $1s \rightarrow 4s$ and crest ($1s \rightarrow 4p$) transitions. The $Fe^{3+}/\Sigma Fe$ ratios determined from linear combinations of end-member spectra ($Fe^{3+}/\Sigma Fe$ ~0 and ~1) were found to deviate significantly from the Mössbauer values. This may indicate the susceptibility of this method either to errors arising from the treatment of the background or to changes in Fe^{2+} or Fe^{3+} coordination with the $Fe^{3+}/\Sigma Fe$ ratio. The general applicability of any XANES calibration for determining oxidation states is limited by variations in the Fe coordination environment, which affects both the intensity and energy of spectral features. Thus previous calibrations based on mineral spectra are not applicable to silicate glasses. Nevertheless, systematic trends in spectral features suggest that $Fe^{3+}/\Sigma Fe$ values may be obtained from XANES spectra, with an accuracy comparable to Mössbauer spectroscopy, by reference to empirical calibration curves derived from compositionally similar standards.

INTRODUCTION

Fe is the most common element in the Earth that exhibits a variable oxidation state, occurring as both Fe^{2+} and Fe^{3+} in minerals and magmas. The $Fe^{3+}/\Sigma Fe$ ratio of geological samples can be used as an indicator of the redox conditions (or oxygen fugacity, f_{O_2}) under which a mineral or melt formed. The oxidation state can be used to infer details about the origin of a magma, and also affects physical and chemical properties such as melt structure, viscosity, the behavior of volatile components, and the temperature and composition of crystallizing phases (Osborn 1959; Hamilton and Anderson 1967; Mysen and Virgo 1989; Carmichael and Ghiorso 1990; Carmichael 1991; Mysen 1991).

The geochemical properties of Fe^{2+} and Fe^{3+} differ so much that they are often treated as though they were different elements. However, modern methods of chemical analysis generally do not distinguish oxidation states; this is particularly a problem with microanalytical techniques such as the electron microprobe and laser ablation inductively coupled plasma mass spectrometry (LA-ICP-MS). Ideally, supplementary methods for identifying oxidation state ratios are required. Various techniques for determining $Fe^{3+}/\Sigma Fe$ have been reviewed by Delaney et al. (1998). These include wet chemical analysis, Mössbauer spectroscopy, and a variety of methods that utilize absorption or emission associated with core-electronic transitions (absorption edges), such as X-ray photoelectron spectroscopy (XPS), electron microprobe studies of $L\alpha,\beta$ peaks (see also Höfer et al. 1994; Fialin et al. 2001), electron energy loss spectroscopy (EELS) (van Aken et al. 1998, 1999; Garvie and Buseck 1998), and X-ray absorption near edge structure (XANES) spectroscopy. Wet chemical analysis and Mössbauer spectroscopy, in general, determine $Fe^{3+}/\Sigma Fe$ ratios of bulk samples. Some degree of spatial resolution is available with the Mössbauer milliprobe, but the analytical scale (>50 μm spot size) is over an order of magnitude larger than that achievable by the electron microprobe and acquisition times can be prohibitive (McCammon et al. 1991; McCammon et al. 2001). In contrast, many of the absorption edge methods are well suited for use at the microanalytical scale. For example, EELS, which uses the characteristic Fe^{2+} and Fe^{3+} peaks of the *L* and *M* edge spectra, is capable of nanometer spatial resolution using a transmission

* E-mail: andrew.berry@anu.edu.au
†Present address: Department of Physics, University of Kelaniya, Kelaniya, Sri Lanka.

electron microscope (TEM); although it is difficult to select specific regions for study (e.g., melt inclusions), since sample preparation involves either crushing or ion-beam thinning to produce electron transmitting sections. XPS experiments are complicated by surface sensitivity and the need for ultra-high vacuum (UHV) techniques. *K*-edge XANES spectroscopy, however, can be undertaken in air, only requires a polished surface, and is capable of the micron spatial resolution required for many geological applications. XANES spectroscopy also has potential for the in situ determination of oxidation states in silicate melts, data that could not be obtained by Mössbauer spectroscopy.

Previous work has demonstrated the potential of *K*-edge XANES spectroscopy for the quantitative estimation of $Fe^{3+}/\Sigma Fe$ ratios in silicate and oxide minerals (Bajt et al. 1994; Delaney et al. 1996, 1998; Dyar et al. 1998, 2001, 2002; Wilke et al. 2001). It is difficult or impractical to determine $Fe^{3+}/\Sigma Fe$ ratios from ab initio modeling of the spectra and instead, determinations depend on the empirical comparison of spectral features with calibration curves prepared from known standards. In most cases, standards consist of minerals with known $Fe^{3+}/\Sigma Fe$ ratios, or physical mixtures of minerals for which intermediate spectra are expected to correspond to linear combinations of the end-members (Wilke et al. 2001). Since features in XANES spectra are strongly dependent on the coordination geometry, it is unlikely that such an approach will give accurate results for unknowns in which the Fe coordination is significantly different from that of the standard. In the case of glasses, Fe may exist in a variety of coordination environments (possibly 4-, 5-, and 6-coordinate for each valence state) with variable site distributions.

Here we investigate the quantitative determination of $Fe^{3+}/\Sigma Fe$ ratios in a silicate glass by XANES spectroscopy. XANES spectra were recorded for a series of 13 anorthite-diopside eutectic glasses (quenched melts) containing 1 wt% $^{57}Fe_2O_3$ prepared at 1409 °C over a $\log f_{O_2}$ range from ~ –13 (fully reduced) to ~ +5 (fully oxidized). The $Fe^{3+}/\Sigma Fe$ ratios of these samples were determined previously by Mössbauer spectroscopy (Jayasuriya et al., in prep.) and are summarized in Figure 1a. The oxidation state ratio was confirmed to be related to f_{O_2} by the expected exponent of 0.25, i.e., $\log[Fe^{3+}/Fe^{2+}] = 0.25\log f_{O_2} + C$ (where $C = \log K$) (Figure 1b). By studying a series in which the $Fe^{3+}/\Sigma Fe$ ratio was varied at closely spaced intervals from ~ 0 to ~ 1, fitting procedures could be optimized and any systematic errors identified and eliminated. The resulting uncertainty in the $Fe^{3+}/\Sigma Fe$ ratio for an individual sample is much smaller than if that sample had been studied in isolation. For the Mössbauer analyses, we have established empirically that $\sigma(Fe^{3+}/\Sigma Fe) = 0.01$ (Jayasuriya et al., in prep.). Features in the XANES spectra could then be referenced to the Mössbauer results in order to determine their dependence on the $Fe^{3+}/\Sigma Fe$ ratio. This allows the suitability, precision, and accuracy of methods for extracting $Fe^{3+}/\Sigma Fe$ ratios from XANES spectra to be determined and compared. The pre-edge centroid energy, the energy of the main absorption edge, the derivative areas of the $1s \rightarrow 4s$ (shoulder) and absorption crest transitions, and linear combinations of end-member spectra ($Fe^{3+}/\Sigma Fe \sim 0$ and 1) for both the pre-edge and total edges, were investigated as possible methods of calibration.

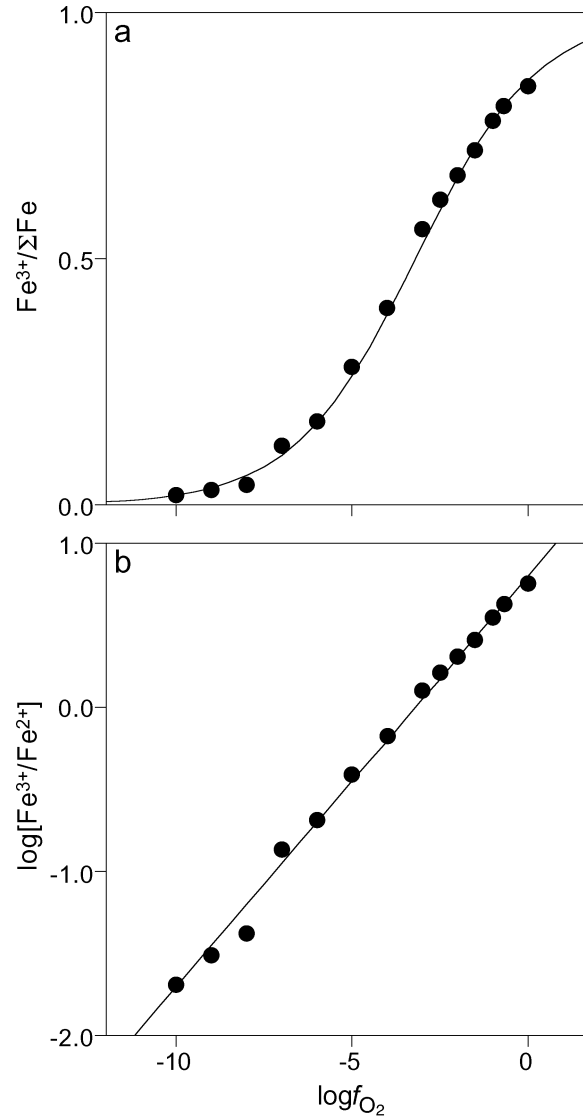

FIGURE 1. Fe oxidation state ratios determined previously by Mössbauer spectroscopy for the series of glasses studied here by XANES spectroscopy. (**a**) $Fe^{3+}/\Sigma Fe$, and (**b**) $\log[Fe^{3+}/Fe^{2+}]$, as a function of oxygen fugacity (f_{O_2}). The fit to the data uses the ideal exponent of 0.25 and in (**b**) has the form $\log[Fe^{3+}/Fe^{2+}] = 0.25 \log f_{O_2} + C$.

XANES SPECTROSCOPY OF Fe^{2+} AND Fe^{3+}

The Fe *K* absorption edge comprises features that have been simplistically identified as transitions to bound states; $1s \rightarrow 3d$ (pre-edge), $1s \rightarrow 4s$ (shoulder), and $1s \rightarrow 4p$ (edge crest) (Shulman et al. 1976; Waychunas et al. 1983). These features (in particular the edge-crest) can also be described as transitions to delocalized or continuum states, which allows multiple scattering modeling of the XANES region (Paris and Tyson 1994; Farges et al. 1997). The energy separations between the transitions correspond to the bound state spectroscopic levels of the $Z + 1$ free ion. The $Z + 1$ model describes the electronic configuration of an ion, *Z*, following promotion of a core 1*s* electron to an excited bound state. The established method for

determining the $Fe^{3+}/\Sigma Fe$ ratio from the *K* absorption edge is the energy of the $1s \rightarrow 3d$ pre-edge transition. This feature shifts to higher energy with increasing $Fe^{3+}/\Sigma Fe$ (Bajt et al. 1994). The number of transitions to ligand field final states comprising the $1s \rightarrow 3d$ feature can be predicted by a d^{n+1} crystal field model where the electron involved in the transition is added to the number of *d* electrons in the Fe oxidation state, e.g., a d^{6+1} configuration for Fe^{2+} (Calas and Petiau 1983). The final states for both Fe^{2+} and Fe^{3+} in various spin states and coordination geometries can be determined from the electron occupancy of the *d*-orbital set (Westre et al. 1997). The energy of these states can also be calculated by ligand field theory. Pre-edges for single oxidation state materials can be fit using the theoretically predicted number of electronic transitions and an appropriate transition line shape (Calas and Petiau 1983). In general terms, four transitions are expected for $^4Fe^{2+}$, three for $^6Fe^{2+}$, and two for $^6Fe^{3+}$, and $^4Fe^{3+}$, although usually only two transitions are needed to model $^4Fe^{2+}$ and one for $^4Fe^{3+}$ (Wilke et al. 2001). Spectra have also been reported for trigonal bipyramidal $^5Fe^{2+}$ in grandidierite as a spectroscopic model for this coordination environment in glasses and melts (Farges 2001; Wilke et al. 2001).

The $1s \rightarrow 3d$ feature may derive from both electric quadrupole and vibronic (dynamic) or ligand field induced (static) electric dipole transitions. The angular dependence of polarized experiments (Dräger et al. 1988) and density functional theory (Westre et al. 1997) can be used to determine the relative contribution of each mechanism. Electric quadrupole transitions are typically up to 100 times weaker than those enabled by the electric dipole mechanism. Electric dipole transitions to 3*d* states are forbidden but gain intensity by mixing with 4*p* orbitals to which electric dipole transitions are allowed. This 3*d*-4*p* mixing is enhanced for coordination environments of low symmetry. As a result, quadrupolar transitions are important for centrosymmetric sites, giving rise to weak pre-edge features, whereas in other cases (no inversion centre) more strongly allowed electric dipole transitions dominate the intensity. Thus transitions for tetrahedrally coordinated Fe are more intense than those for Fe in an octahedral environment. Orbital mixing also enables $1s \rightarrow 4s$ transitions. The $1s \rightarrow 4s$ is more intense than the $1s \rightarrow 3d$ due to the smaller energy separation (larger mixing) between the 4*s* and 4*p* compared to the 3*d* and 4*p* levels (Shulman et al. 1976).

A detailed understanding of the electronic structure and coordination geometry of Fe in a material allows the number, energy, and intensity of component transitions to the 3*d* manifold to be predicted, in good agreement with the results of high resolution experiments (Westre et al. 1997). In some cases, this has enabled intensity not derived from transitions to 3*d* states to be identified and removed from determinations of the centroid energy (Calas and Petiau 1983; Wilke et al. 2001). However, it is difficult to model the transitions and resulting pre-edge for mixed oxidation states or a range of coordination environments. Instead $Fe^{3+}/\Sigma Fe$ ratios may be determined with reference to calibration standards.

The first attempts to use the $1s \rightarrow 3d$ pre-edge energy to determine the $Fe^{3+}/\Sigma Fe$ ratio found a linear peak energy shift with oxidation state for fayalite, magnetite, and hematite (Bajt et al. 1994). The resulting calibration curve was found to give $Fe^{3+}/\Sigma Fe$ ratios in good agreement with Mössbauer and wet chemical results for a range of minerals in which both Fe^{2+} and Fe^{3+} are located exclusively at octahedral sites (Delaney et al. 1996, 1998). It has also been used to determine the Fe^{3+} content of oxidized olivine, micas, and silicates in metapelites (Dyar et al. 1998, 2001, 2002). The accuracy was estimated to be ±0.05–0.15 $Fe^{3+}/\Sigma Fe$ depending upon the unknown. An analogous calibration determined specifically for garnet has an accuracy of ±0.03–0.10 (Dyar et al. 2002). This simple linear calibration may be appropriate for the majority of rock-forming minerals, in which Fe occupies an octahedral site, but is not expected to be applicable for minerals containing Fe at other sites, or for the range of coordination environments found in a glass.

Wilke et al. (2001) investigated a large range of Fe-bearing model compounds containing Fe^{2+} and Fe^{3+} in a variety of coordination geometries. The centroid of the Fe $1s \rightarrow 3d$ transition was shown to vary smoothly for mechanical mixtures of $^4Fe^{2+}$, $^4Fe^{3+}$, $^6Fe^{2+}$, and $^6Fe^{3+}$. The centroid for a particular oxidation state occurs at constant energy irrespective of the coordination geometry. Mixtures of oxidation states would correlate linearly with the centroid energy if the intensity of the Fe^{2+} and Fe^{3+} transitions were equal. This is generally not the case since transition intensities are strongly dependent upon the site symmetry. The result is a weighting of the centroid energy toward the oxidation state with the higher transition intensity and curvature of the calibration curve.

An alternative method of quantifying $Fe^{3+}/\Sigma Fe$ uses linear combinations of features in reference materials (Manceau et al. 1992). Galoisy et al. (2001) determined the oxidation state ratio of glasses from the relative contribution of Fe^{2+} (augite glass equilibrated near Fe/FeO) and Fe^{3+} ($^4Fe^{3+}$ and $^6Fe^{3+}$ in YIG; yttrium iron garnet) pre-edge components to the glass pre-edge. Experimental spectra could be reproduced with about 90% confidence but errors of up to 25% relative to the results of wet chemical analysis were noted. These discrepancies were attributed to either the pre-edge extraction or differences in Fe site geometry between the unknowns and model compounds.

The $Fe^{3+}/\Sigma Fe$ ratio in glasses has also been calibrated by fitting the pre-edge to pseudo-Voigt components regarded as characteristic of each oxidation state (Bonnin-Mosbah et al. 2001). The area of the Fe^{3+} curve relative to the total, for a series of glasses for which the oxidation state ratio had been determined by titration, was then used to define a calibration curve against which the results for unknown micron-sized melt inclusions could be compared. The error in these measurements would appear to be at least ±0.1 $Fe^{3+}/\Sigma Fe$.

In this paper the trends in several spectral features for a series of samples with accurately known $Fe^{3+}/\Sigma Fe$ ratios are investigated. The objective of this, and planned future work on an extended range of compositions, is to identify a method of calibration which is sensitive to changes in oxidation state but relatively unaffected by variations in bonding and coordination environment.

EXPERIMENTAL METHODS

Glasses were prepared from reagent grade MgO, Al_2O_3, SiO_2, and $CaCO_3$ in the approximate stoichiometry of the anorthite-diopside eutectic (42% $CaAl_2Si_2O_8$ + 58% $CaMgSi_2O_6$ by weight; 50.47(19)% SiO_2, 15.12(10)% Al_2O_3, 10.46(12)% MgO, and 23.94(16)% CaO) to which was added 1 wt% Fe_2O_3 con-

taining 93.5 at% ^{57}Fe. The molten oxides were equilibrated in a gas mixing vertical tube furnace at 1409 °C using H_2/CO_2, CO/CO_2, CO_2/O_2, and O_2 to control the f_{O_2} at values of $\log f_{O_2}$ between ~ –13 ($Fe^{3+}/\Sigma Fe \sim 0$) and 0. Samples were suspended in the furnace on loops of wire made of metals which inhibit alloying with Fe, and are stable under the f_{O_2} conditions of the experiment; Re for $\log f_{O_2} \leq -8$, Ir for $\log f_{O_2} = -6$, and Pt for $\log f_{O_2} \geq -5$. After at least 24 h melts were quenched in water to give transparent homogeneous glasses. The chosen composition typically produces high quality glasses and there was no evidence of quench microcrystals by either optical microscopy or back-scattered electron imaging. Further details of this type of sample preparation can be found in O'Neill and Eggins (2002). A sample with $Fe^{3+}/\Sigma Fe \sim 1$ was prepared by equilibrating the oxides in a sealed platinum capsule containing 20 wt% PtO_2 at 1.1 GPa and 1400 °C for 4 h using a piston-cylinder apparatus. Under these conditions PtO_2 breaks down to Pt producing O_2 at a partial pressure equal to the confining pressure. From the equation of state of pure O_2 (Belonoshko and Saxena 1991) this corresponds to $\log f_{O_2} = +4.8$. The glasses were powdered in order to prepare homogeneous sections ($\phi \sim 10$ mm) for Mössbauer spectroscopy, with the remainder being pressed into pellets ($\phi \sim 3$ mm) for the XANES experiments. Synthetic fayalite and hematite, and natural magnetite, were powdered and diluted with BN for use as reference mineral standards.

Mössbauer spectra were recorded at room temperature, and at 4.2 K for selected samples, using a constant acceleration Mössbauer spectrometer (Jing et al. 1992) with a rhodium matrix ^{57}Co source and a standard α-Fe foil for calibration. The spectrum of the fully reduced sample comprises an asymmetric doublet which was fit by a distribution of overlapping elementary doublets of Lorentzian shape. In contrast, the spectrum of the fully oxidized sample was fit by a single broadened symmetric doublet and several broadened sextets. Intermediate spectra were fit using initial parameter values equal to those obtained for either the reduced or oxidized samples. The $Fe^{3+}/\Sigma Fe$ ratio was determined from the sub-spectral areas of the Fe^{2+} and Fe^{3+} components. Similar results were obtained for both the room temperature and 4.2 K spectra indicating equal recoil-free fractions for both Fe^{2+} and Fe^{3+}. Since Fe^{2+} and Fe^{3+} sub-spectral areas are highly correlated significant uncertainties are usually associated with $Fe^{3+}/\Sigma Fe$ ratios determined for isolated samples. For this series of samples, the uncertainty can be estimated from a linear regression of the data to $\log[Fe^{3+}/Fe^{2+}] = 0.25\log f_{O_2} + C$ in which the reduced χ^2 value is constrained to be unity, i.e., the scatter from an ideal fit for the whole data set gives an indication of the accuracy of the component points. This suggests $\sigma(Fe^{3+}/\Sigma Fe) = 0.01$. Full details of the spectral modeling and error estimation are given in Jayasuriya et al. (in preparation). The error in our $Fe^{3+}/\Sigma Fe$ values determined by Mössbauer spectroscopy is significantly less than usually quoted. This results from fitting many systematically varying samples (including the pure end-members), which allows possible errors in the assignment of sub-spectral components to be minimized.

Fe *K*-edge XANES spectra were recorded in fluorescence mode at the Australian National Beamline Facility, beamline 20B (bending magnet) at the 2.5 GeV Photon Factory (KEK, Tsukuba, Japan). The excitation energy was selected using a water-cooled Si (111) channel-cut crystal monochromator located 11 m from the light source. The resulting energy bandpass of the monochromator is 1.87 eV at the Fe *K* edge, which when coupled with the Fe*K*α core-hole width of 1.25 eV indicates a spectral energy resolution of 2.2 eV. The beam size of 2 mm (horizontal) × 0.5 mm (vertical) was controlled with a slit assembly 13 m from the source. The energy was calibrated by defining the first derivative peak of Fe foil to be 7112.0 eV and the spectrum of one sample was recorded at regular intervals to determine the energy reproducibility. Fluorescence was measured using a Canberra GL0110S ten-element Ge array detector. The signal from each array element was passed from the detector, via a Canberra model 2026XA spectroscopy amplifier (shaping time 0.25 μs), to a Canberra model 2030 single-channel analyzer, which was set to pass the Fe*K*α signal to the counting electronics. Peak counts due to Fe*K*α photons were typically around 15 000 s^{-1} per element, with the distance of the detector from the sample set so as to limit the total incoming count rate to less than 10^5 s^{-1} per element, which is within the linear response range of the detector system. The fluorescence was normalized to the incident beam flux monitored by an ionization chamber with a 30 cm path length containing 30% N_2 in He. Spectra were recorded from 7103–7293 eV using a 0.1 eV step size for the pre-edge region (7108–7118 eV), a 0.25 eV step size for the baseline (7103–7108 eV) and edge (7118–7138 eV) regions, and a 2.5 eV step above 7138 eV. Within each region data were collected for a constant number of ionization chamber counts. Typical count times were around 3.5 s per point for the pre-edge and 2.5 s per point elsewhere, for a total scan time of 20–25 min. All spectra were recorded in a single experimental session. Following each scan, the signals from the ten detector elements were normalized and averaged to produce the reduced data for further analysis.

The sizes of the aperture ($\phi \sim 10$ mm) in the Mössbauer experiment and the slit/beam (2 × 0.5 mm) in the XANES experiment are sufficiently large for the analysis volumes of each technique to be representative of the bulk material. Thus, for a homogeneous glass/powder, the results of the two experiments should be directly comparable.

RESULTS

A selection of Fe *K*-edge XANES spectra is shown in Figure 2a. A constant baseline was first subtracted followed by normalization to the average absorption coefficient between 7200 and 7300 eV. It was not necessary to further correct the spectra for background since the intensity was effectively constant with energy over this range. The first derivative of the spectra are shown in Figure 2b.

As shown in Figure 3, the pre-edge and edge region of the XANES spectra comprise features which may be attributed to

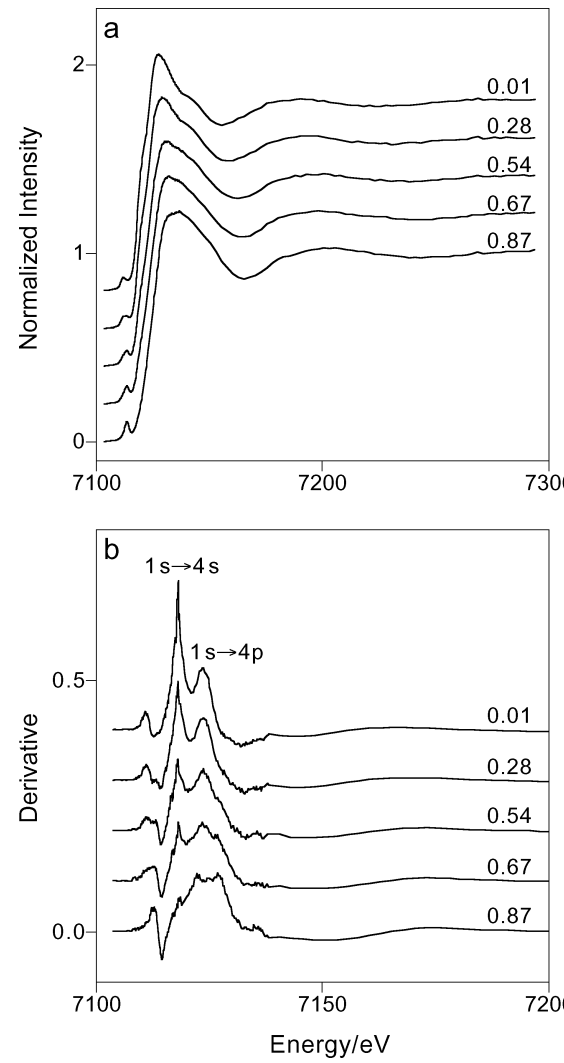

FIGURE 2. (**a**) Selected Fe *K*-edge XANES spectra, and (**b**) the corresponding first derivative spectra, *dI*/*dE*, for the $Fe^{3+}/\Sigma Fe$ ratios given. Features in (**b**), the integrated areas of which are plotted in Figure 7, are labeled according to the bound state electronic transitions with which they are associated. The spectra are offset for clarity.

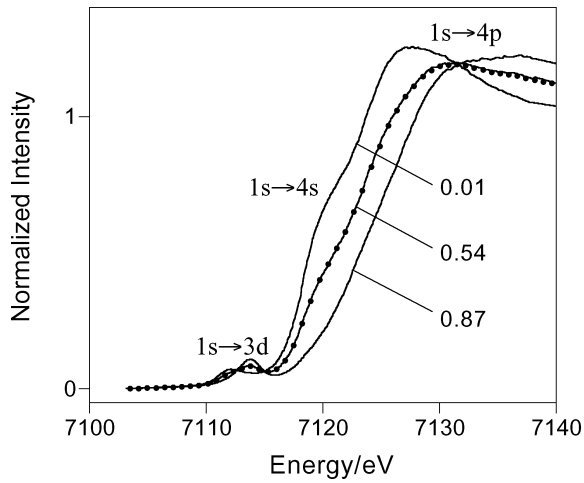

FIGURE 3. Fe *K*-edge XANES spectra for samples with $Fe^{3+}/\Sigma Fe$ values of 0.01, 0.54, and 0.87. Features assigned as transitions between bound electronic states are indicated. The best fit to the $Fe^{3+}/\Sigma Fe$ = 0.54 sample from a linear combination of the other two spectra (42% $Fe^{3+}/\Sigma Fe$ = 0.01 and 58% $Fe^{3+}/\Sigma Fe$ = 0.87) is indicated by the small circles.

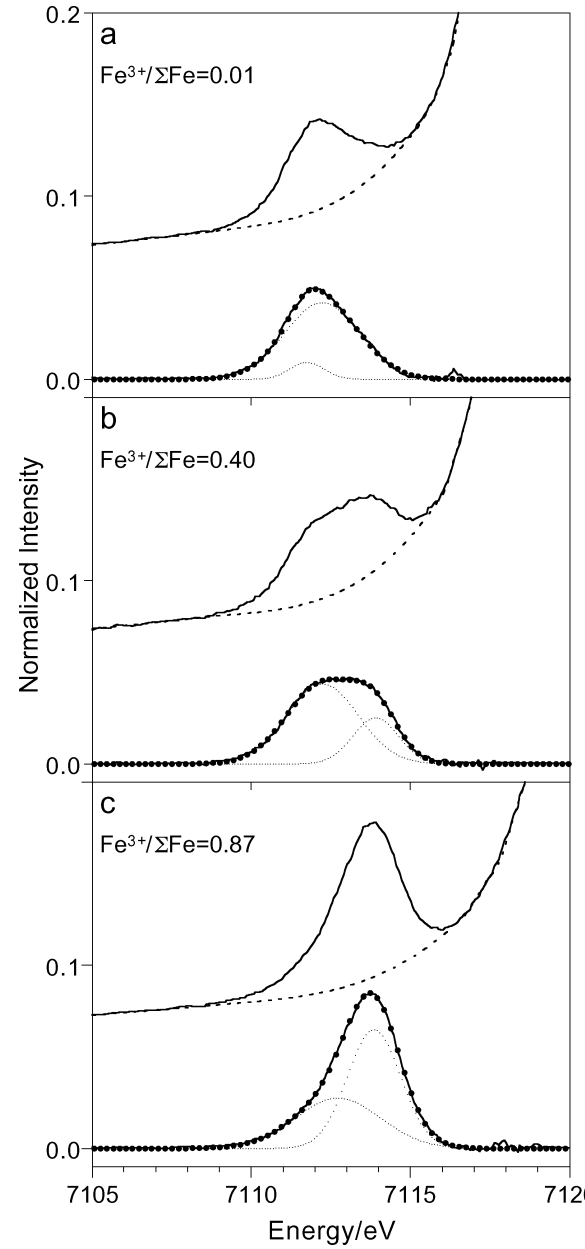

FIGURE 4. The $1s \rightarrow 3d$ pre-edge feature superimposed on the tail of the main absorption edge for samples with $Fe^{3+}/\Sigma Fe$ values of (**a**) 0.01, (**b**) 0.40, and (**c**) 0.87. The raw data and background corrected (extracted) pre-edges (solid lines), spline fit to the background (dashed line), fit to the extracted pre-edge (small circles), and Gaussian components of the fit (dotted lines), are shown in each case.

transitions between bound electronic states. In general terms transitions of this type shift to higher energy with increasing oxidation state (Wong et al. 1984; Sutton et al. 1993; Bajt et al. 1994). Smooth spectral trends were observed across the $Fe^{3+}/\Sigma Fe$ series, except for the fully oxidized sample which exhibits a lower intensity pre-edge and higher energy *K*-edge than expected. This presumably reflects changes in Fe coordination associated with the different pressure of preparation.

The $1s \rightarrow 3d$ pre-edge transition is superimposed on the tail of the main absorption edge (Figs. 3 and 4). It comprises several components corresponding to transitions to different 3*d* crystal field levels. The number of transitions depends upon both the oxidation state and the coordination geometry (Westre et al. 1997). However, neither Fe^{2+} nor Fe^{3+} coordination geometries are well characterized in silicate melts or glasses. Fe^{3+} and Fe^{2+} can be both octahedrally and tetrahedrally coordinated, and there is also evidence for fivefold coordination, differences with composition, and differences between coordination in the melt and that quenched in at the glass transition temperature (Brown et al. 1995). For a mixture of oxidation states and resulting coordination geometries multiple crystal field transitions are to be expected, but it is not practical, or necessary for the purposes of this work, to attempt an accurate model of the 3*d* electronic structure. Instead, the centroid of the transition intensity is determined and treated as an empirical variable for quantifying the oxidation state ratio.

The energy centroid of the $1s \rightarrow 3d$ transition is strongly affected by how the background is modeled (Fig. 4). The sloping region below the pre-edge is fit well by a straight line which was subtracted as a baseline. A spline function was then used to define a smooth curve through the absorption edge from several eV above, to the now flat baseline below the pre-edge. This curve was constrained to be positive at all times and to be equivalent to the baseline before joining with it. A selection of the resulting effective baselines and extracted pre-edges are shown in Figure 4. Previous studies have used spline (Wilke et al. 2001), arc-tangent (Calas and Petiau 1983; Galoisy et al. 2001; Manceau et al. 1992), second-order polynomial (Bajt et al. 1994; Delaney et al. 1996, 1998), and pseudo-Voigt (Westre et al. 1997) functions to model the baseline under the pre-edge.

The choice of function is probably not significant for a relative study in which a set of samples and reference materials are treated consistently, but may be important when comparing absolute results with those in the literature. In the present study, the resulting smooth baseline interpolations shown in Figure 4 appear reasonable although there is a subjective component to the fit, somewhat constrained by the behavior of the spline function. In particular, the tightness of curvature can produce a significant weighting to the extracted pre-edge. Thus the absolute value of the energy centroid for a given compound may vary between studies due to the nature of the fluorescence background, the function chosen to model the background under the pre-edge, and the choice of "best fit".

After subtraction of the edge background, the pre-edge feature was fit to two, or occasionally three, Gaussians (Fig. 4). The spectral lineshape converged to Gaussian when the Gaussian and Lorentzian contributions to a pseudo-Voigt function were allowed to vary, despite the expected Lorentzian profile of the electronic transitions (Calas and Petiau 1983). This is a consequence of the beamline resolution (insufficient to resolve the core-hole lifetime broadening responsible for the Lorentzian shape) and the effect of overlapping bands derived from multiple site geometries. The peaks comprising the pre-edge multiplet should all have the same width, however, this variable was not constrained. The actual number and functional form of the peaks used to model the pre-edge is not important providing the resulting fit accurately describes the intensity distribution, thus allowing the centroid to be determined, i.e., the experimental resolution and peak fitting method is irrelevant for an empirical approach. The centroid is the energy of half the total integrated intensity of the fit to the pre-edge. The glass centroid values, together with those for the three mineral standards (fayalite, magnetite, and hematite), are given in Table 1. Magnetite can be used as an energy reference standard relative to which future experiments, with a possibly different energy calibration or data treatment to this work, may be compared.

The extracted pre-edge spectra shown in Figure 5 exhibit a shift to higher energy with increasing $Fe^{3+}/\Sigma Fe$ ratio. The data emphasize the smooth, systematic progression in both energy and intensity across the series. The relationship between the pre-edge centroid and $Fe^{3+}/\Sigma Fe$ ratio determined by Mössbauer spectroscopy is shown in Figure 6. The $Fe^{3+}/\Sigma Fe$ values obtained from the equation of best-fit ("theoretical" Mössbauer), determined by fitting the Mössbauer data to the theoretical expression $\log[Fe^{3+}/Fe^{2+}] = 0.25\log f_{O_2} + C$, are used instead of the raw values to minimize the Mössbauer experimental error for individual points. The experimental error or reproducibility is indicated by the three data points for the sample with $Fe^{3+}/\Sigma Fe = 0.54$ and the four data points for magnetite (Fig. 6 and Table 1), determined from spectra recorded at various times in the same experimental session. These replicate points are shown in all the following figures demonstrating correlations between spectral features and the $Fe^{3+}/\Sigma Fe$ ratio.

Three other spectral features were also investigated for suitability to quantify the oxidation state. The energy of the main absorption edge at a height of 0.9 as a function of the $Fe^{3+}/\Sigma Fe$ ratio is shown in Figure 7a. The value of 0.9 was chosen in an attempt to determine the energy near the edge jump (normalized to 1.0) while minimizing any distortions arising from transitions associated with the crest. Intensity changes and shifts in features associated with the absorption edge suggest that these may also be useful for quantifying the oxidation state,

TABLE 1. The centroid energy and integrated intensity of the $1s \rightarrow 3d$ pre-edge feature for glass samples prepared at 1409 °C and various f_{O_2} values, and three mineral standards

Sample	$\log f_{O_2}$	$1s \rightarrow 3d$ Centroid Energy (eV)	$1s \rightarrow 3d$ Intensity	$Fe^{3+}/\Sigma Fe$ Mössbauer (experimental) ±0.01	(theoretical) ±0.00	$Fe^{3+}/\Sigma Fe$ XANES ±0.02	Δ
fev19	–12.9	7112.137	0.135	0.000	0.001	0.039	0.038
fev2	–10.9	7112.116	0.141	0.025	0.007	0.023	0.016
fev5	–7.9	7112.214	0.131	0.043	0.061	0.085	0.024
fev12	–5.9	7112.344	0.156	0.171	0.176	0.160	–0.016
fev6	–4.9	7112.454	0.150	0.280	0.276	0.225	–0.051
fev15	–3.9	7112.723	0.169	0.399	0.403	0.378	–0.025
fev8	–3.0	7113.004	0.182	0.558	0.541	0.546	0.005
"	"	7113.005	0.185	"	"	0.547	0.006
"	"	7113.001	0.188	"	"	0.544	0.003
fev10	–2.4	7113.116	0.192	0.624	0.616	0.611	–0.005
fev11	–2.0	7113.244	0.213	0.667	0.673	0.686	0.013
fev13	–1.5	7113.339	0.205	0.717	0.731	0.742	0.011
fev14	–1.0	7113.443	0.219	0.784	0.782	0.802	0.020
fev9	0.0	7113.527	0.228	0.851	0.865	0.852	–0.013
d60*	+4.8	7113.725	0.246	1.000	0.990	0.967	–0.023
fayalite	–	7112.006	0.100	–	0.000	–0.037†	–0.037†
magnetite	–	7113.569	0.340	–	0.667	0.876	0.209
"	–	7113.539	0.333	–	0.667	0.858	0.191
"	–	7113.588	0.337	–	0.667	0.887	0.220
"	–	7113.576	0.329	–	0.667	0.880	0.213
hematite	–	7114.623	0.366	–	1.000	1.492†	0.492

Notes: Replicate measurements obtained from three different spectra of sample fev8, and four different spectra of magnetite, are given. The "experimental" $Fe^{3+}/\Sigma Fe$ ratios were determined by fitting the Mössbauer spectra. The "theoretical" Mössbauer values were calculated for each $\log f_{O_2}$ value using the equation of best fit obtained from a weighted non-linear least-squares regression of the "experimental" data to $\log(Fe^{3+}/Fe^{2+}) = 0.25 \log f_{O_2} + C$ (cf. Fig. 1). The $Fe^{3+}/\Sigma Fe$ (XANES) values were calculated from the centroid energy using the linear calibration shown in Figure 6. Δ is the difference between the XANES and "theoretical" Mössbauer $Fe^{3+}/\Sigma Fe$ ratios. All uncertainties are one standard deviation.

* 1.1 GPa and 1400 °C.

† Physically meaningless values.

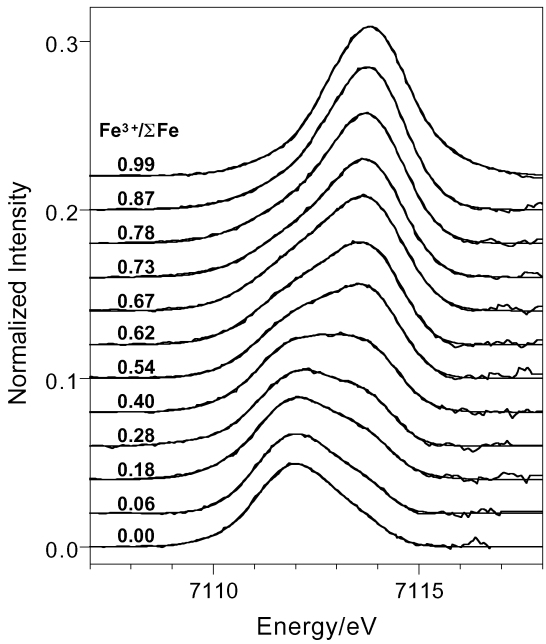

FIGURE 5. The extracted $1s \rightarrow 3d$ pre-edge features showing systematic changes in both energy and intensity with the indicated $Fe^{3+}/\Sigma Fe$ ratio. The raw data and fits are superimposed to emphasize the quality of the fits from which the centroid values were determined.

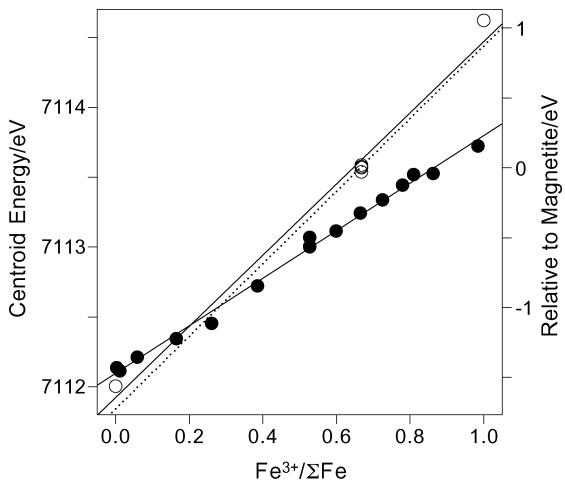

FIGURE 6. The $1s \rightarrow 3d$ pre-edge centroid energy for the silicate glass samples (•) and fayalite, magnetite, and hematite (o) as a function of the $Fe^{3+}/\Sigma Fe$ ratio determined by Mössbauer spectroscopy. Solid lines represent the best fit to the glass and reference mineral data. The dotted line corresponds to the calibration expression of Dyar et al. (1998).

despite the potential for strong coordination effects due to the radial extent of the component 4*s* and 4*p* final states (Delaney et al. 1996). The shoulder on the absorption edge corresponding to the forbidden $1s \rightarrow 4s$ transition (Fig. 3) appears as a peak in the derivative spectrum (Fig. 2b). The area of this derivative peak has been used to quantify Cr oxidation states in similar silicate glasses (Berry and O'Neill, in prep.). A second

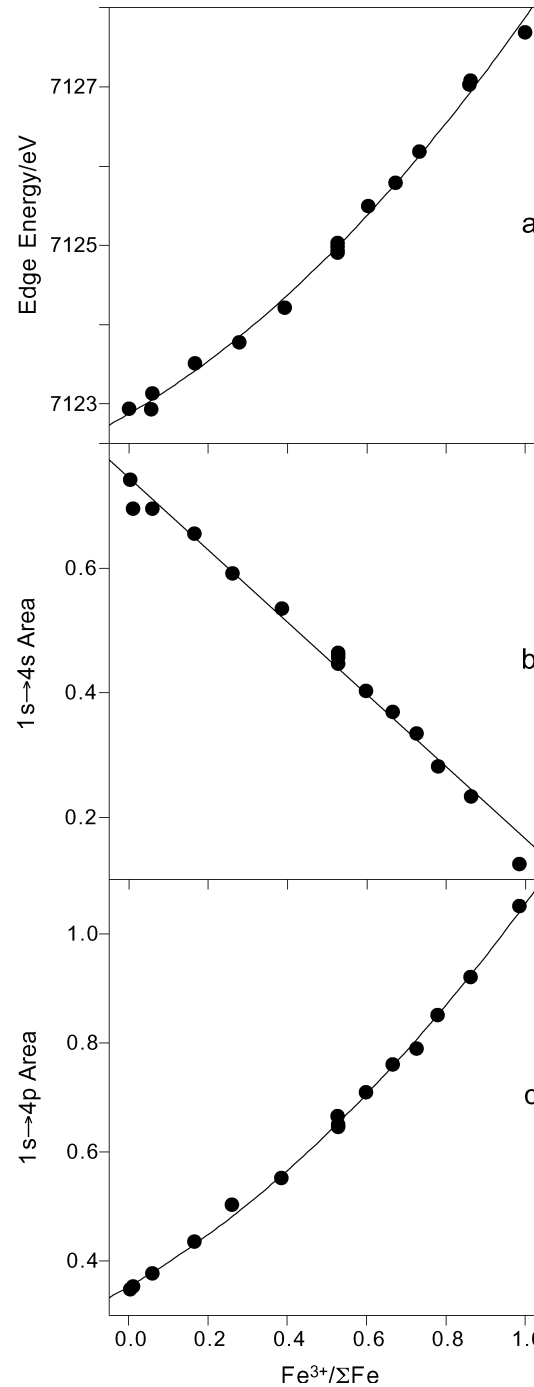

FIGURE 7. Alternative calibration methods; trends in (**a**) the energy of the main absorption edge at a normalized height of 0.9, (**b**) the area of the derivative peak associated with the $1s \rightarrow 4s$ transition (Fig. 2b), and (**c**) the area of the derivative peak associated with the absorption crest ($1s \rightarrow 4p$), as a function of the $Fe^{3+}/\Sigma Fe$ ratio determined by Mössbauer spectroscopy.

peak, attributed to the $1s \rightarrow 4p$ transition, is associated with the crest of the main edge. The areas of the derivative peaks for both the $1s \rightarrow 4s$ (7114.7–7121.3 eV) and $1s \rightarrow 4p$ (7121.3–7134.7 eV) transitions as a function of the $Fe^{3+}/\Sigma Fe$ ratio are shown in Figures 7b and 7c.

Discussion

The key aspect of this work is the acquisition of spectra for a series of glasses for which the $Fe^{3+}/\Sigma Fe$ ratios range from 0 to 1 and are accurately known from a concurrent Mössbauer study (Fig. 1). This allows changes in the spectra that depend on the $Fe^{3+}/\Sigma Fe$ ratio to be identified. The correlation between the $Fe^{3+}/\Sigma Fe$ ratio and the energy of the centroid of the pre-edge transition for both the glasses, and the reference minerals fayalite ($Fe^{3+}/\Sigma Fe = 0$), magnetite ($Fe^{3+}/\Sigma Fe = 0.67$), and hematite ($Fe^{3+}/\Sigma Fe = 1$), are shown in Figure 6. Although other minerals may be more suitable as model compounds, these three were chosen since they define a linear trend (Bajt et al. 1994) which has been used to determine $Fe^{3+}/\Sigma Fe$ ratios of various other minerals in good agreement with available wet chemical and Mössbauer values (Delaney et al. 1996, 1998; Dyar et al. 1998, 2001, 2002). Figure 6 shows that the results of the present work closely correlate with the calibration expression of Dyar et al. (1998) referenced to our sample of magnetite. It should be noted that essentially identical centroid energies were obtained by fitting the pre-edge to either single (as in Bajt et al. 1994) or multiple Gaussians (as in this work). Although this calibration is not claimed to be suitable for all systems, it would appear to give reasonable results for octahedrally coordinated Fe (Dyar et al. 1998, 2001, 2002). This apparent accuracy is perhaps fortuitous since a substantial component (~30–40%) of the hematite pre-edge intensity does not derive from $1s \rightarrow 3d$ transitions (Wilke et al. 2001). The calibration is, however, clearly inappropriate for the glass samples which exhibit a much smaller ΔeV(centroid) for $\Delta Fe^{3+}/\Sigma Fe = 1$. The differences in the calibration can be attributed to not only the anomalous pre-edge intensity in hematite, but also to differences in the Fe site which affects the intensity of the component pre-edge transitions and hence the centroid energy. Calibrations specific to different glass compositions, such as shown here, are required to account for the number and variation of Fe coordination environments. The $Fe^{3+}/\Sigma Fe$ ratios calculated from the best fit to the XANES data are given in Table 1, together with the differences between these values and those determined from the theoretical fit to the Mössbauer data. For the glasses, the standard deviation of the difference values ($\sigma = 0.02$) indicates an uncertainty in the XANES $Fe^{3+}/\Sigma Fe$ ratio of ± 0.02 (one standard deviation), assuming the "theoretical" Mössbauer ratios are without error. The differences between the XANES and "experimental" Mössbauer (± 0.01) ratios are also consistent with a XANES error of $\sim \pm 0.02$. As expected, large errors are associated with the $Fe^{3+}/\Sigma Fe$ ratios determined for the mineral standards using the glass calibration.

The approximately linear relationship for the glass samples in Figure 6 is not necessarily expected. The energy centroid of the $1s \rightarrow 3d$ transition is constant to first order for a given oxidation state, since the ligands simply split the crystal field levels (degeneracy weighted) about a barycentre energy. The centroid and barycentre will be equivalent when the transition probability to each of the split components is identical. This relationship has been observed for a wide range of minerals with Fe in different coordination environments (Wilke et al. 2001). The effective barycentre energy will vary linearly for mixtures of oxidation states; however, changes in oxidation state are invariably associated with changes in the coordination environment. This produces differences in the transition probability for Fe^{2+} and Fe^{3+}; the $1s \rightarrow 3d$ transition gains increasing intensity with decreasing centro-symmetry. As a result of this intensity weighting the centroid energy is expected to vary non-linearly with oxidation state. For example, summing together equal amounts of very intense and very weak components will produce a centroid similar to that of the intense component rather than at the net barycentre energy mid-way between the two. The degree of curvature, or deviation from linearity, is dependent upon the difference in transition intensity of the two end-members. This effect has been demonstrated for physical mixtures of Fe (Wilke et al. 2001) and Ti minerals (Farges et al. 1996). It is clear from Figure 5 and Table 1 that the relative intensities of the $1s \rightarrow 3d$ feature in the most reduced and oxidized samples are different. Indeed, the $Fe^{3+}/\Sigma Fe$ ratios calculated from summing varying fractions of the end-member pre-edges underestimate the amount of Fe^{3+}. For example, the fit to a sample with $Fe^{3+}/\Sigma Fe = 0.673$ is shown in Figure 8. This excellent fit is a scaled linear combination of 33% of the Fe^{2+} (fev2; 99% Fe^{2+}) and 67% of the "Fe^{3+}" (fev9; 86.5% Fe^{3+} + 13.5% Fe^{2+}) pre-edges. The shape of the pre-edge could only be reproduced using this end-member ratio coupled with a scaling multiplier of 1.07. The $Fe^{3+}/\Sigma Fe$ ratio calculated in this way is 0.581, which differs from the Mössbauer value by 0.092. The sample with $Fe^{3+}/\Sigma Fe = 0.865$ was used for the Fe^{3+} "end-member" due to the effect of pressure on the spectrum of the fully oxidized sample. As expected, the correlation between centroid energy and the $Fe^{3+}/\Sigma Fe$ ratios determined by pre-edge fitting deviates significantly from the linear relationship obtained using the $Fe^{3+}/\Sigma Fe$ values found by Mössbauer spectroscopy. A fit to give the correct $Fe^{3+}/\Sigma Fe$ ratio would require the intensity of the Fe^{2+} and Fe^{3+} end-member pre-edges to be scaled by 1.4 and 0.95, respectively. Wilke et al. (2001) compared the pre-edge spectra of a 50:50 mix of variously coordinated Fe^{2+} and Fe^{3+} minerals with those calculated from summing the spectra of the pure compounds. The experimental and calculated spectra are expected to be identical and differences were attributed to errors in the baseline subtraction. Such errors may result from changes in the pre-edge background due to both the shift with oxidation state of the main edge position relative to the pre-edge and differences in the transitions comprising the edge (such as the $1s \rightarrow 4s$ shoulder observed here for reduced samples). Thus, a constant baseline subtraction procedure may not always produce a correctly extracted $1s \rightarrow 3d$ pre-edge. While this is not a problem for an empirical calibration it is important for $Fe^{3+}/\Sigma Fe$ determinations referenced to individual spectra. In this work, the need to scale the intensity of either the resultant linear combination or the end-members to achieve a satisfactory reproduction of the pre-edge indicates the susceptibility of this type of treatment to baseline and normalization errors. The baselines of either the Fe^{2+} or

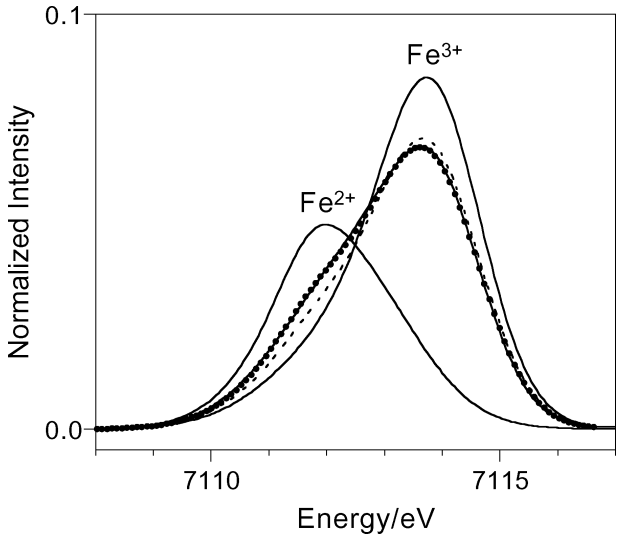

FIGURE 8. The fits to the $1s \rightarrow 3d$ extracted pre-edge features for the Fe^{2+} ($Fe^{3+}/\Sigma Fe = 0.01$) and Fe^{3+} ($Fe^{3+}/\Sigma Fe = 0.87$) "end-member" samples. The pre-edge fit for the sample with $Fe^{3+}/\Sigma Fe = 0.67$ (solid line) is also shown together with the best fit (small circles) using a scaled linear combination of the other two spectra (33% $Fe^{3+}/\Sigma Fe$ = 0.01 and 67% $Fe^{3+}/\Sigma Fe = 0.87$). The expected pre-edge for the combination of end-member spectra for which $Fe^{3+}/\Sigma Fe = 0.67$ is indicated by the dashed line.

Fe^{3+} end-member spectra could be poorly modeled and the source of the error in both the intensities and the $Fe^{3+}/\Sigma Fe$ values determined by pre-edge fitting. It is also possible that the intensities of the Fe^{2+} and Fe^{3+} components do not vary linearly with $Fe^{3+}/\Sigma Fe$ (discussed below). The use of end-member spectra to determine the oxidation state ratio of an unknown is hence susceptible to significant errors.

The energy and intensity of the extracted pre-edge features are strongly dependent upon how the main absorption edge is extrapolated under the pre-edge to represent the baseline. Thus the quantitative determination of $Fe^{3+}/\Sigma Fe$ ratios from pre-edge centroids requires reference to standards in which the baseline is treated in the same way as for the unknowns. The calibration curves derived here are hence not necessarily suitable for calculating $Fe^{3+}/\Sigma Fe$ ratios from centroids quoted in the literature. This means that an absolute calibration of pre-edge centroid energy against oxidation state (even referenced to a standard such as magnetite) may be an unrealistic expectation. The most accurate method for determining the $Fe^{3+}/\Sigma Fe$ ratio of a glass would be to compare the spectrum of the unknown to a series of standards, with the same chemical composition, equilibrated over a range of f_{O_2}s. In the absence of an independent determination, the $Fe^{3+}/\Sigma Fe$ ratio of the standards could be estimated from the empirical relationship between $\log(Fe^{3+}/Fe^{2+})$, $\log f_{O_2}$, temperature, and composition, determined by Sack et al. (1980) (or its subsequent modifications and refinements).

The main absorption edge comprises several features, such as the $1s \rightarrow 4s$ shoulder and crest ($1s \rightarrow 4p$) transitions, both of which appear to vary systematically with oxidation state (Fig. 3). Fits of these additional features, and the entire edge region, to Gaussian curves were found to be too poorly constrained to be reliable. Thus, attempts were made to model the edge as a linear combination of end-member spectra, similar to that described above for the pre-edge feature. An example is shown in Figure 3 where the $Fe^{3+}/\Sigma Fe = 0.541$ sample is plotted along with the fit obtained using 48% of the Fe^{2+} (fev2; 99% Fe^{2+}) and 67% of the "Fe^{3+}" (fev9; 86.5% Fe^{3+} + 13.5% Fe^{2+}) spectra. The fit is excellent over the entire range for which data was collected (~7100–7300 eV). This edge fitting method gives $Fe^{3+}/\Sigma Fe = 0.453$, a difference of 0.088 compared with the value determined by Mössbauer spectroscopy. The reason for this difference is not obvious since, in contrast with the pre-edge fits, only a simple linear baseline subtraction is required, and the spectra shown in Figure 2a exhibit similar and constant fluorescence with energy from 7200–7300 eV. Inappropriate modeling of the baseline would, therefore, appear unlikely. For both the pre-edge and total edge, fitting of end-member spectra to an intermediate composition results in lower $Fe^{3+}/\Sigma Fe$ ratios than expected. A possible explanation for the discrepancy (and the intensity problem with the pre-edge fits) is that the coordination environment, and thus transition intensity, of Fe^{2+} and Fe^{3+} in a mixed oxidation state sample is different to that in the end members. It is possible that at the high temperatures of the melt, while the $Fe^{3+}/\Sigma Fe$ ratio is constant, the rate of electron exchange between different Fe cations is sufficiently fast (compared to relaxation of the melt structure), that discrete Fe^{2+} and Fe^{3+} environments, similar to those in the end-member spectra, do not exist and that an average coordination structure occurs which is retained on quenching. The intensity and centroid of transitions to this average state in the glass will thus not be represented by a summation of the spectra for transitions to pure Fe^{2+} and Fe^{3+} glasses. This could explain the error in the results of the pre-edge and total edge fits since both comprise transitions with some dependence on the coordination environment. It may also explain the linear correlation of the centroid energy with $Fe^{3+}/\Sigma Fe$ ratio, which is unexpected given the different intensities of the Fe^{2+} and Fe^{3+} pre-edge transitions.

Several alternative calibration methods are shown in Figure 7. In Figure 7a, the shift of the main absorption edge to higher energy with increasing $Fe^{3+}/\Sigma Fe$ ratio is illustrated. The edge represents a superposition of the atomic absorption (dependent upon oxidation state) with transitions to various bound and delocalized states, the intensity of which are strongly dependent on the coordination geometry. Intense edge transitions can introduce large apparent edge shifts (Shulman et al. 1976). For example, the edge energy of Cu^{+} and Cu^{2+} can be shifted by ~ 5 eV due to the presence of an intense $1s \rightarrow 4p$ transition in some Cu^{+} compounds (Fulton et al. 2000). The relationship between edge energy and the $Fe^{3+}/\Sigma Fe$ ratio thus depends upon the energy and intensity of the component transitions and the curved relationship shown in Figure 7a is not unexpected. The area of features in the derivative spectrum (Fig. 2b) is a convenient construct for quantifying information contained in the absorption edge (Figs. 7b and 7c). For example, the shoulder ($1s \rightarrow 4s$) on the edge appears as a peak in the derivative spectrum, the intensity or area of which is easily quantified and varies with $Fe^{3+}/\Sigma Fe$ (Fig. 7b). As the edge comprises multiple transitions, which may independently change intensity or energy with the $Fe^{3+}/\Sigma Fe$ ratio, the integral range chosen to de-

fine a particular feature is unlikely to sample a single transition. Thus the range selected is somewhat arbitrary and there is little physical meaning associated with the area values; however, this is not important for an empirical calibration approach. The complexity of the edge and crest electronic structures also suggests that simple linear correlations would not necessarily be expected. In all cases (Fig. 7a-c) the smooth trends with $Fe^{3+}/\Sigma Fe$ ratio indicate that quantitative results may be expected for compositionally similar unknowns from calibrations of this type.

In general terms, any method that relies on transition intensities is subject to error due to possible changes in the Fe coordination. The coordination strongly affects the number of transition components and their intensity. All the calibration methods investigated for determining $Fe^{3+}/\Sigma Fe$ from XANES spectra are potentially influenced by the Fe environment, either directly through the intensity of a feature or indirectly as a result of an apparent energy shift due to the relative weighting of different component transitions. Measurements of the energy rather than the intensity of features minimise the effect of the coordination environment.

Incorporating the details of the Fe coordination into modelling of the pre-edge or edge transitions is only possible for spectra recorded with a high energy resolution and when the coordination environment is well defined. This latter point does not apply to Fe in glasses. However, the instrument resolution and modeling of the transitions comprising XANES features are not important for determining accurate oxidation state ratios when a feature can be referenced to an empirical calibration curve. Correlations of spectral features with changes in the $Fe^{3+}/\Sigma Fe$ ratio determined by Mössbauer spectroscopy suggests a number of possible calibration methods. In particular, the energy centroid of the $1s \rightarrow 3d$ transition was found to be linearly correlated with the $Fe^{3+}/\Sigma Fe$ ratio. The general applicability of any calibration for glasses is uncertain and will depend upon how the intensity of transitions associated with each oxidation state vary with melt composition, pressure, and glass transition temperature. These variables may modify the melt structure, the Fe coordination, and the preference of the melt for stabilising either Fe^{2+} or Fe^{3+}. The smooth correlation of features with $Fe^{3+}/\Sigma Fe$ ratio suggests that accurate f_{O_2} values for an unknown may be determined with reference to a series of standards. This work indicates the potential of XANES spectroscopy to determine the oxidation state of Fe in silicate glasses (and hence the redox conditions under which a melt equilibrated) with an accuracy comparable to that attained by Mössbauer spectroscopy.

ACKNOWLEDGMENTS

Part of this work was performed at the Australian National Beamline Facility with support from the Australian Synchrotron Research Program, which is funded by the Commonwealth of Australia under the Major National Research Facilities Program. K.D.J. was funded in part by a grant from the Australian Research Council. We thank D.R. Scott for sample preparation, and S. Sutton and M. Wilke for detailed reviews.

REFERENCES CITED

Bajt, S., Sutton, S.R., and Delaney, J.S. (1994) X-ray microprobe analysis of iron oxidation states in silicates and oxides using X-ray absorption near edge structure (XANES). Geochimica et Cosmochimica Acta, 58, 5209–5214.

Belonoshko, A. and Saxena, S.K. (1991) A molecular-dynamics study of the pressure-volume-temperature properties of supercritical fluids 2. CO_2, CH_4, CO, O_2, and H_2. Geochimica et Cosmochimica Acta, 55, 3191–3208.

Brown, G.E. Jr., Farges, F., and Calas, G. (1995) X-ray scattering and X-ray spectroscopy studies of silicate melts. In J.F. Stebbins, P.F. McMillan, and D.B. Dingwell, Eds., Structure Dynamics and Properties of Silicate Melts, Reviews in Mineralogy, 32, p. 317–410. Mineralogical Society of America, Washington, D.C.

Bonnin-Mosbah, M., Simionovici, A.S., Métrich, N., Duraud, J.-P., Massare, D., and Dillmann, P. (2001) Iron oxidation states in silicate glass fragments and glass inclusions with a XANES micro-probe. Journal of Non-Crystalline Solids, 288, 103–113.

Calas, G. and Petiau, J. (1983) Coordination of iron in oxide glasses through high-resolution *K*-edge spectra: information from the pre-edge. Solid State Communications, 48, 625–629.

Carmichael, I.S.E. (1991) The redox states of basic and silicic magmas: a reflection of their source region. Contributions to Mineralogy and Petrology, 106, 129–141.

Carmichael, I.S.E. and Ghiorso, M.S. (1990) The effect of oxygen fugacity on the redox state of natural liquids and their crystallizing phases. In J. Nicholls and J.K. Russell, Eds., Modern Methods of Igneous Petrology: Understanding Magmatic Processes, Reviews in Mineralogy, 24, p. 191–212. Mineralogical Society of America, Washington, D.C.

Delaney, J.S., Bajt, S., Sutton, S.R., and Dyar, M.D. (1996) In situ microanalysis of $Fe^{3+}/\Sigma Fe$ in amphibole by x-ray absorption near edge structure (XANES) spectroscopy. In M.D. Dyar, C. McCammon, and M.W. Schaefer, Eds., Mineral spectroscopy: a tribute to Roger G. Burns, p. 165–171. The Geochemical Society, Houston.

Delaney, J.S., Dyar, M.D., Sutton, S.R., and Bajt, S. (1998) Redox ratios with relevant resolution: solving an old problem by using the synchrotron microXANES probe. Geology, 26, 139–142.

Dräger, G., Frahm, R., Materlik, G., and Brümmer, O. (1988) On the multipole character of the X-ray transitions in the pre-edge structure of Fe K absorption spectra. Physica Status Solidi B, 146, 287–294.

Dyar, M.D., Delaney, J.S., Sutton, S.R., and Schaefer, M.W. (1998) Fe^{3+} distribution in oxidized olivine: a synchrotron micro-XANES study. American Mineralogist, 83, 1361–1365.

Dyar, M.D., Delaney, J.S., and Sutton, S.R. (2001) Fe XANES spectra of iron-rich micas. European Journal of Mineralogy, 13, 1079–1098.

Dyar, M.D., Lowe, E.W., Guidotti, C.V., and Delaney, J.S. (2002) Fe^{3+} and Fe^{2+} partitioning among silicates in metapelites: A synchrotron micro-XANES study. American Mineralogist, 87, 514–522.

Farges, F. (2001) Crystal chemistry of iron in natural grandidierites: an X-ray absorption fine-structure spectroscopy study. Physics and Chemistry of Minerals, 28, 619–629.

Farges, F., Brown Jr., G.E., and Rehr, J.J. (1996) Coordination chemistry of Ti (IV) in silicate glasses and melts: I. XAFS study of titanium coordination in oxide model compounds. Geochimica et Cosmochimica Acta, 60, 3023–3038.

Farges, F., Brown Jr., G.E., and Rehr, J.J. (1997) Ti *K*-edge XANES studies of Ti coordination and disorder in oxide compounds: comparison between theory and experiment. Physical Review B, 56, 1809–1819.

Fialin, M., Wagner, C., Métrich, N., Humler, E., Galoisy, L., and Bézos, A. (2001) $Fe^{3+}/\Sigma Fe$ vs. Fe$L\alpha$ peak energy for minerals and glasses: Recent advances with the electron microprobe. American Mineralogist, 86, 456–465.

Fulton, J.L., Hoffmann, M.M., and Darab, J.G. (2000) An X-ray absorption fine structure study of copper(I) chloride coordination structure in water up to 325 °C. Chemical Physics Letters, 330, 300–308.

Galoisy, L., Calas, G., and Arrio, M.A. (2001) High-resolution XANES spectra of iron in minerals and glasses: structural information from the pre-edge region. Chemical Geology, 174, 307–319.

Garvie, L.A.J. and Buseck, P.R. (1998) Ratios of ferrous to ferric iron from nanometre-sized areas in minerals. Nature, 396, 667–670.

Hamilton, D.L. and Anderson, G.M. (1967) Effects of water and oxygen pressures on the crystallization of basaltic magmas. In H.H. Hess and A. Poldervaart, Eds., Basalts, p. 445–482. Interscience Publishers, New York.

Höfer, H.E., Brey, G.P., Schulz-Dobrick, B., and Oberhänsli, R. (1994) The determination of the oxidation state of iron by the electron microprobe. European Journal of Mineralogy, 6, 407–418.

Jing, J., Campbell, S.J., and Pellegrino, J. (1992) A stand-alone Mössbauer spectrometer based on the MC 68008 microprocessor. Measurement Science and Technology, 3, 80–84.

Manceau, A., Gorshkov, A.I., and Drits, V.A. (1992) Structural chemistry of Mn, Fe, Co, and Ni in manganese hydrous oxides: Part I. Information from XANES spectroscopy. American Mineralogist, 77, 1133–1143.

McCammon, C.A., Chaskar, V., and Richards, G.G. (1991) A technique for spatially resolved Mössbauer spectroscopy applied to quenched metallurgical slags. Measurement Science and Technology, 2, 657–662.

McCammon, C.A., Griffin, W.L., Shee, S.R., and O'Neill, H.S.C. (2001) Oxidation during metasomatism in ultramafic xenoliths from the Wesselton kimberlite, South Africa: implications for the survival of diamond. Contributions to Mineralogy and Petrology, 141, 287–296.

Mysen, B.O. (1991) Relations between structure, redox equilibria of iron, and properties of magmatic liquids. In L.L. Perchuk and I. Kushiro, Eds., Physical Chemistry of Magmas, Advances in Physical Geochemistry, 9, p. 41–98. Springer-Verlag, New York.

Mysen, B.O. and Virgo, D. (1989) Redox equilibria, structure, and properties of Fe-bearing aluminosilicate melts: relationships among temperature, composition, and oxygen fugacity in the system Na_2O-Al_2O_3-SiO_2-Fe-O. American Mineralogist, 74, 58–76.

O'Neill, H.S.C. and Eggins, S.M. (2002) The effect of melt composition on trace element partitioning: an experimental investigation of the activity coefficients of FeO, NiO, CoO, MoO_2 and MoO_3 in silicate melts. Chemical Geology, 186, 151–181.

Osborn, E.F. (1959) Role of oxygen pressure in the crystallization and differentiation of basaltic magma. American Journal of Science, 257, 609–647.

Paris, E. and Tyson, T.A. (1994) Iron site geometry in orthopyroxene: multiple scattering calculations and XANES study. Physics and Chemistry of Minerals, 21, 299–308.

Sack, R.O., Carmichael, I.S.E., Rivers, M., and Ghiorso, M.S. (1980) Ferric-ferrous equilibria in natural silicate liquids at 1 bar. Contributions to Mineralogy and Petrology, 75, 369–376.

Shulman, R.G., Yafet, Y., Eisenberger, P., and Blumberg, W.E. (1976) Observation and interpretation of x-ray absorption edges of iron compounds and proteins. Proceedings of the National Academy of Science, 73, 1384–1388.

Sutton, S.R., Jones, K.W., Gordon, B., Rivers, M.L., Bajt, S., and Smith, J.V. (1993) Reduced chromium in olivine grains from lunar basalt 15555: X-ray absorption near edge structure (XANES). Geochimica et Cosmochimica Acta, 57, 461–468.

van Aken, P.A., Liebscher, B., and Styrsa, V.J. (1998) Quantitative determination of iron oxidation states in minerals using Fe $L_{2/3}$-edge electron energy-loss near-edge structure spectroscopy. Physics and Chemistry of Minerals, 25, 323–327.

van Aken, P.A., Styrsa, V.J., Liebscher, B., Woodland, A.B., and Redhammer, G.J. (1999) Microanalysis of $Fe^{3+}/\Sigma Fe$ in oxide and silicate minerals by investigation of electron energy-loss near-edge structures (ELNES) at the Fe $M_{2,3}$ edge. Physics and Chemistry of Minerals, 26, 584–590.

Waychunas, G.A., Apted, M.J., and Brown Jr., G.E. (1983) X-ray K-edge absorption spectra of Fe minerals and model compounds: near edge structure. Physics and Chemistry of Minerals, 10, 1–9.

Westre, T.E., Kennepohl, P., DeWitt, J.G., Hedman, B., Hodgson, K.O., and Solomon, E.I. (1997) A multiplet analysis of Fe K-edge 1s $\rightarrow$3d pre-edge features of iron complexes. Journal of the American Chemical Society, 119, 6297–6314.

Wilke, M., Farges, F., Petit, P.-E., Brown Jr., G.E., and Martin, F. (2001) Oxidation state and coordination of Fe in minerals: an Fe *K*-XANES spectroscopic study. American Mineralogist, 86, 714–730.

Wong, J., Lytle, F.W., Messmer, R.P., and Maylotte, D.H. (1984) K-edge absorption spectra of selected vanadium compounds. Physical Review B, 30, 5596–5609.

MANUSCRIPT RECEIVED AUGUST 6, 2002
MANUSCRIPT ACCEPTED FEBRUARY 25, 2003
MANUSCRIPT HANDLED BY SIMONA QUARTIERI